

DISK–JET CONNECTION IN ACTIVE SUPERMASSIVE BLACK HOLES IN THE STANDARD ACCRETION DISK REGIME

YOSHIYUKI INOUE¹, AKIHIRO DOI¹, YASUYUKI T. TANAKA², MAREK SIKORA³, GREGORZ M. MADEJSKI⁴

¹Institute of Space and Astronautical Science JAXA, 3-1-1 Yoshinodai, Chuo-ku, Sagami-hara, Kanagawa 252-5210, Japan

²Hiroshima Astrophysical Science Center, Hiroshima University, 1-3-1 Kagamiyama, Higashi-Hiroshima, Hiroshima 739-8526, Japan

³Nicolaus Copernicus Astronomical Center, Bartycka 18, 00-716 Warsaw, Poland

and

⁴Kavli Institute for Particle Astrophysics and Cosmology, SLAC National Accelerator Laboratory, Stanford University, 2575 Sand Hill Road M/S 29, Menlo Park, CA 94025, USA

¹e-mail: yinoue@astro.isas.jaxa.jp

ABSTRACT

We study the disk-jet connection in supermassive black holes by investigating the properties of their optical and radio emissions utilizing the SDSS-DR7 and the NVSS catalogs. Our sample contains 7017 radio-loud quasars with detection *both* at 1.4 GHz and SDSS optical spectrum. Using this radio-loud quasar sample, we investigate the correlation among the jet power (P_{jet}), the bolometric disk luminosity (L_{disk}), and the black hole mass (M_{BH}) in the standard accretion disk regime. We find that the jet powers correlate with the bolometric disk luminosities as $\log P_{\text{jet}} = (0.96 \pm 0.012) \log L_{\text{disk}} + (0.79 \pm 0.55)$. This suggests that the jet production efficiency of $\eta_{\text{jet}} \simeq 1.1_{-0.76}^{+2.6} \times 10^{-2}$ assuming the disk radiative efficiency of 0.1 implying low black hole spin parameters and/or low magnetic flux for radio-loud quasars. But it can be also due to dependence of the efficiency on geometrical thickness of the accretion flow which is expected to be small for quasars accreting at the disk Eddington ratios $0.01 \lesssim \lambda \lesssim 0.3$. This low jet production efficiency does not significantly increase even if we set the disk radiative efficiency of 0.3. We also investigate the fundamental plane in our samples among P_{jet} , L_{disk} , and M_{BH} . We could not find a statistically significant fundamental plane for radio-loud quasars in the standard accretion regime.

Keywords: accretion, accretion disks - black hole physics - galaxies: active - galaxies: jets - quasars: supermassive black holes

1. INTRODUCTION

Relativistic jets launched by supermassive black holes (SMBHs), so-called as active galactic nuclei (AGNs), are known as the most energetic particle accelerators in the universe. Because of their gigantic power, those jets would affect the fate of galaxies, and also galaxy clusters (e.g. Fabian 2012). However, the launching mechanism of a collimated relativistic jet from a black hole system is a long standing problem in astrophysics.

Theoretically, the Blandford-Znajek (BZ) mechanism (Blandford & Znajek 1977) is believed as the plausible explanation for the jet launch. In the BZ mechanism, the jet power is extracted by the rotation of BHs with the support of the magnetic fields threading the central BH. Recent numerical simulations confirm this process

as a plausible and efficient jet power extraction mechanism (e.g. Komissarov et al. 2007; Tchekhovskoy et al. 2010, 2011; McKinney et al. 2012; Takahashi et al. 2016).

Observational evidence for the jet production mechanisms in AGNs are not clear yet. A possible and important key to understand the jet launching mechanism is to measure spins of the nuclear BHs which is a key parameter for the jet. For example, Sikora et al. (2007) argued that spin parameter would determine the AGN radio loudness distribution. Although various spin measurement methods have been proposed in literature (e.g. Moriyama & Mineshige 2015, and references therein), spin determination of active SMBHs is currently uncertain (e.g. Martínez-Sansigre & Rawlings 2011; Brennen et al. 2011; King et al. 2013; Liu et al. 2015).

It is also possible to investigate the jet production mechanisms from observations by probing the relation between disk inflow and jet outflow, because a part of infall materials to the central BH are ejected as the jet outflow and those accreting material also accumulate the magnetic field in the vicinity of the SMBHs. For example, recent systematic spectral analysis for luminous blazars by Ghisellini et al. (2014) shows the jet power is slightly larger than the power of accreting plasma, although the results depend on the assumptions on the pair fraction and the minimum energy of electrons (e.g. Inoue & Tanaka 2016; Pjanka et al. 2016). On the contrary to blazars, in radio quasars, the efficiency of jet energy extraction from rest energy of accreted masses, i.e. the jet production efficiency, is not well understood yet.

Here, after the discovery of quasars, their radio emission is found to be associated with a presence of luminous optical emission lines (Baade & Minkowski 1954; Osterbrock 1977; Grandi & Osterbrock 1978). A correlation between radio jet luminosities and disk emission line luminosities in radio galaxies is later found (e.g. Baum & Heckman 1989; Saunders et al. 1989; Rawlings et al. 1989; Rawlings & Saunders 1991; Zirbel & Baum 1995; Willott et al. 1999; Buttiglione et al. 2010; Koziel-Wierzbowska & Stasińska 2011; Sikora et al. 2013). The correlation of radio jet luminosities and various optical emissions has been studied in more detail as the mass of the nuclear BH became available (e.g. Woo & Urry 2002). The BH mass provide fundamental information for the jet study such as the Eddington luminosity and its ratio.

Using the BH mass information, BH systems have been found to have a fundamental plane among mass, disk luminosity, and jet power (e.g. Terashima & Wilson 2003; Merloni et al. 2003; Maccarone et al. 2003). Merloni et al. (2003) established the fundamental plane in stellar mass and supermassive BHs using BH mass, jet core radio luminosity, and disk X-ray luminosity. With ~ 150 BH system samples, they found that the radio core luminosity is correlated with both the mass and the X-ray luminosity of the disk. However, AGN disk luminosity is known to be dominated not in X-ray but in optical (e.g., Elvis et al. 1994). X-ray emission is reprocessed optical emission via Comptonization processes in hot accretion disk coronae (e.g., Katz 1976; Pozdniakov et al. 1977; Sunyaev & Titarchuk 1980). Moreover, as recent studies suggest that the fundamental plane exist only for low accretion rate BH systems (see e.g. Merloni & Heinz 2008; Plotkin et al. 2012), a fundamental plane for objects accreting at high rates is not well established.

The Sloan Digital Sky Survey (SDSS; York et al. 2000) has facilitated studies of AGNs in optical with wide and deep field surveys (e.g. Shen et al. 2011). SDSS

has detected 166583 quasars in optical covering about a quarter of the sky (Pâris et al. 2014). For the radio data, using Very Large Array (VLA), the NRAO VLA Sky Survey (NVSS) has observed the entire sky north of -40 deg declination at 1.4 GHz down to ~ 2.5 mJy (Condon et al. 1998). NVSS has detected $\gtrsim 1.8$ million sources. In this paper, we study the relation among the jet power (P_{jet}), the bolometric disk luminosity (L_{disk}), and the black hole mass (M_{BH}) using quasar samples detected *both* in SDSS and NVSS which will allow us to investigate the disk–jet connection in the largest ever radio quasar sample.

This paper is organized as follows. In Section 2, we introduce the sample used in our analysis. In Section 3, the relation between accretion inflows and jet outflows is presented. SMBH fundamental planes are discussed in Section 4. Discussion and conclusion is given in Section 5 and Section 6, respectively. Throughout this paper, we adopt the standard cosmological parameters of $(h, \Omega_M, \Omega_\Lambda) = (0.7, 0.3, 0.7)$.

2. SAMPLE

The NVSS was carried out utilizing the VLA radio interferometric telescopes at a frequency of 1.4 GHz (Condon et al. 1998). The NVSS was conducted with the array D configuration which provides a spatial resolution of 45 arcsec (corresponding to the physical size of ~ 76 kpc at $z = 1$). Although this resolution is not as good as that of the Faint Images of the Radio Sky at Twenty-cm (FIRST; Becker et al. 1995) having ~ 5 arcsec (corresponding to the size of ~ 8.5 kpc at $z = 1$), the NVSS resolution secures to measure fluxes of extended sources more accurately (Lu et al. 2007).

The NVSS covers the entire sky north of -40 deg declination ($\sim 33,000$ deg²) and contains over 1.8 million sources down to a limiting flux density of ~ 2.5 mJy. The survey gives astrometric accuracy ranges from 1 arcsec for bright sources to ~ 7 arcsec for faint sources. We extract integrated flux densities from the NVSS catalog to evaluate the whole extended radio flux.

The SDSS is an optical imaging and spectroscopic survey (e.g., York et al. 2000) using a 2.5 m wide-field telescope at the Apache Point Observatory (Gunn et al. 2006). The photometric survey contains five wavelength bands (*ugriz*; Fukugita et al. 1996). The survey covers about a quarter of the sky. A subset of photometric sources are chosen for spectroscopic observation according to the spectral target selection algorithms of SDSS. The survey catalog now contains 166583 quasars (Pâris et al. 2014). Here, Shen et al. (2011) provided detailed spectral properties of the SDSS data release (DR) 7 quasar catalog (Schneider et al. 2010) which contains 105783 quasars brighter than $M_i = -22.0$. In this paper, we utilize the SDSS DR7 quasar catalog provided

by Shen et al. (2011) as we are interested in the spectral properties of quasars.

From the SDSS-DR7 quasar catalog, we extract redshifts, rest-frame 2500 Å fluxes, bolometric luminosities, disk Eddington ratios, and virial BH mass estimates. 2500 Å fluxes at the rest frame were determined from the power-law continuum fit to the spectrum. Bolometric luminosities were computed from continuum luminosities at 5100 Å ($z < 0.7$), 3000 Å ($0.7 \leq z < 1.9$), and 1350 Å ($z \geq 1.9$) using the bolometric luminosity correction factors of 9.26, 5.15, and 3.81 from the spectral energy distribution (SED) templates in Richards et al. (2006). Although various studies report different correction factors (see e.g. Elvis et al. 1994; Richards et al. 2006; Nemmen & Brotherton 2010; Runnoe et al. 2012; Krawczyk et al. 2013), those studies are consistent with in a factor of ~ 2 . We note that this bolometric luminosity includes emission from dust (infrared), accretion disk (optical), and corona (X-ray). In this paper, we approximate this bolometric luminosity equals to the bolometric disk luminosity, since SDSS quasars have $L_{\text{disk},2500\text{\AA}} \gtrsim 10^{44}$ erg s $^{-1}$ where bolometric luminosities are dominated by accretion disks.

BH masses were estimated from single-epoch spectra (virial mass) in the SDSS quasar survey (Shen et al. 2011)¹. Using the continuum luminosity and full width at half-maximum (FWHM), the virial mass estimate is given by

$$\log\left(\frac{M_{\text{BH}}}{M_{\odot}}\right) = a + b \log\left(\frac{\lambda L_{\lambda}}{10^{44} \text{ erg s}^{-1}}\right) + 2 \log\left(\frac{\text{FWHM}}{\text{km s}^{-1}}\right), \quad (1)$$

where a and b are the empirical coefficients calibrated with local AGNs using the reverberation mapping method (e.g. Blandford & McKee 1982; Peterson 1993; Kaspi et al. 2000). Shen et al. (2011) use the line of H β for $z < 0.7$, MgII for $0.7 \leq z < 1.9$, and C $_{\text{IV}}$ for $z \geq 1.9$. The coefficients are as follows: $(a, b) = (0.910, 0.50)$, $(0.740, 0.62)$, and $(0.660, 0.53)$ for H β (Vestergaard & Peterson 2006), MgII (McLure & Dunlop 2004; Shen et al. 2011), and C $_{\text{IV}}$ (Vestergaard & Peterson 2006), respectively.

Shen et al. (2011) matched the DR7 quasar catalog with the FIRST catalog with a matching radius of 30 arcsec. In this paper, we match the NVSS radio sources and the DR7 quasar catalog with a matching radius of 30 arcsec and select the closest sources be-

¹ Spatially resolved kinematics observations are limited to only nearby sources. Various indirect mass measurement methods have been developed such as the reverberation mapping (e.g. Blandford & McKee 1982; Peterson 1993; Kaspi et al. 2000) and the correlation between the optical luminosity and the broad-line-region size (e.g. Kaspi et al. 2000; McLure & Dunlop 2001; Vestergaard 2002).

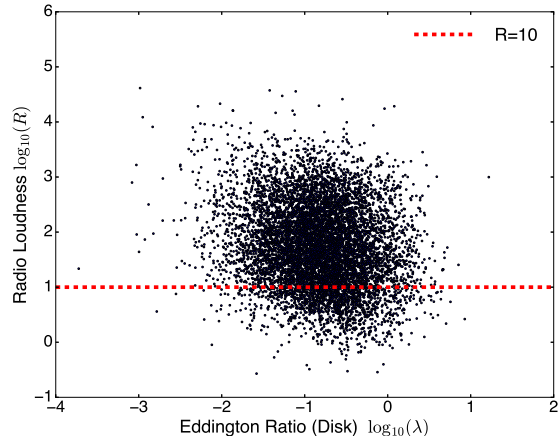


Figure 1. Accretion disk Eddington ratio λ vs. radio loudness R of our SDSS–NVSS quasar sample. $R = 10$ is shown by the dashed line.

tween the catalogs. As we are targeting SDSS detected quasars, the dominant radio quasar population is expected to be Fanaroff–Riley Class II (FR-II; Fanaroff & Riley 1974) whose radio brightest component, so-called hot spot, locates within several hundreds kpc away from the nucleus (e.g., Mullin et al. 2008) which corresponds to ~ 30 arcsec at $z \sim 1$ –3.

Best et al. (2005) matched the SDSS DR2 galaxy catalog and the NVSS catalog out to 3 arcmin. They found that positional offsets between SDSS galaxies and their nearest NVSS source is significant out to 100 arcsec, although they concluded that true associations is expected to be smaller than 15 arcsec. We consider the case for a matching radius of 15 arcsec later at subsection 5.3. Our results do not change even if adopting different matching radiuses.

After the catalog matching, the resulting number of objects detected both in radio and optical is 8436. To examine a luminosity correlation in radio galaxies, we derive the rest-frame radio and optical luminosities as follows. The rest luminosity at a frequency ν_0 in the unit of erg s $^{-1}$ Hz $^{-1}$ is obtained as

$$L_{\nu}(\nu_0) = 4\pi d_L(z)^2 (1+z)^{\alpha-1} F_{\nu}(\nu_0), \quad (2)$$

where $d_L(z)$ is the luminosity distance at a redshift z , α is the spectral index, and F_{ν} is the observed flux. For the radio spectral index (i.e., $F_{\nu} \propto \nu^{-\alpha}$ in the unit of mJy), we assume $\alpha = 0.8$ (Kimball & Ivezić 2008; Sikora et al. 2013). The SDSS DR7 catalog provides the rest-frame flux $F_{\lambda,\text{rest}}$ in the unit of [erg cm $^{-2}$ s $^{-1}$ Å $^{-1}$]. Figure 1 shows the distribution of SDSS–NVSS quasars in the space of the accretion disk Eddington ratio $\lambda \equiv L_{\text{disk}}/L_{\text{Edd}}$ and the radio loudness $R \equiv L_{5 \text{ GHz}}/L_{B\text{-band}}$ (e.g. Sikora et al. 2007). For the optical spectral index, we assume $\alpha = 0.5$ (Richards et al. 2006).

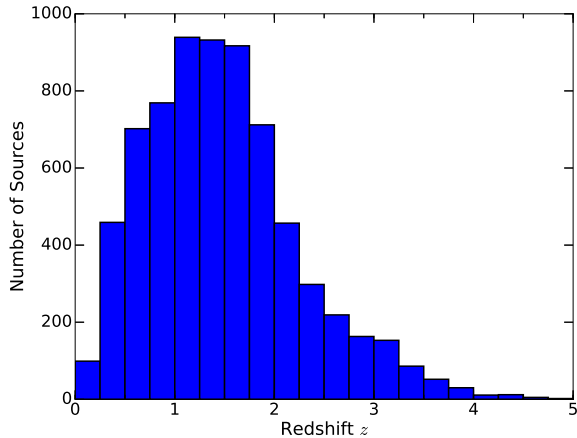


Figure 2. Redshift distribution of the radio-loud SDSS-NVSS quasar sample. 7017 objects are contained.

We are interested in the relation between the jet and the accretion disk, i.e. radio-loud objects. Radio emission from radio-quiet quasars ($R < 10$) is expected to be associated with shocks produced by quasar driven outflows rather than jets (e.g. Zakamska & Greene 2014). To select radio-loud quasars, we select sources having $R \geq 10$ for the main sample which includes 7017 quasars. The redshift distribution of our radio-loud quasar sample is shown in Figure 2. Redshifts of our sample range from 0.077 to 4.922. Majority of the samples ($\sim 87\%$) are at $z \leq 2.5$.

Figure 3 shows the 2500 Å and 1.4 GHz luminosity relation of our SDSS-NVSS radio-loud quasar samples. We need to examine the reliability of the correlation between the optical and radio luminosities. In the flux-limited samples, luminosities of samples can be strongly correlated with redshifts due to the detection limits. This might result in a spurious correlation. To avoid this, we perform a partial correlation analysis (see e.g. Padovani 1992; Ghirlanda et al. 2011; Inoue 2011) to test the correlation between the logarithmic optical and radio luminosities excluding the redshift dependence. The Spearman rank correlation gives $\rho_{\text{or},z} = 0.39$ with the p-value of $< 10^{-10}$ (i.e. the probability of the null hypothesis). Therefore, there is a weak positive correlation between optical and radio luminosities in our radio quasar samples. The correlation analysis results in this paper are summarized in Table 1. The tests are performed using the astronomy survival analysis code ASURV (Lavalley et al. 1992) implemented in the STSDAS package in iraf.

3. RELATION BETWEEN JET OUTFLOW AND ACCRETION DISK INFLOW

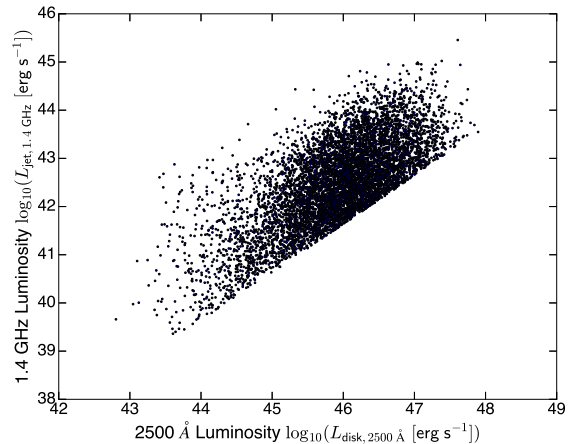


Figure 3. Optical luminosity at 2500 Å vs. radio luminosity at 1.4 GHz of our radio-loud SDSS-NVSS quasar sample ($R \geq 10$).

The jet power is known to be correlated with the radio luminosity (e.g. Willott et al. 1999; O’Sullivan et al. 2011). The empirical relation gives the time-averaged jet power from the extended radio luminosity as (Willott et al. 1999)

$$P_{\text{jet}} = 9.5 \times 10^{46} \left(\frac{f}{10} \right)^{3/2} \left(\frac{L_{151 \text{ MHz}}}{10^{28} \text{ W Hz}^{-1} \text{ sr}^{-1}} \right)^{6/7} [\text{erg s}^{-1}], \quad (3)$$

where f is a parameter accounting for systematic error in the model assumptions. The following parameters are absorbed in the parameter f : the factor accounting for energy loss via the adiabatic expansion, the factor accounting for the bulk and turbulent kinetic energy of the lobe, the energy fraction of radiating particles, the angle between the magnetic field direction and the line-of-sight, the low frequency cutoff in the synchrotron spectrum, the volume filling factor, and deviations from the minimum-energy condition. Willott et al. (1999) constrained as $1 \leq f \lesssim 20$ by using X-ray cavity measurements. In this paper, we set $f = 10$ following the recent X-ray cavity and hot spot studies (Blundell & Rawlings 2000; Godfrey & Shabala 2013). We note the power given in Equation 3 is the time-averaged value.

As we use the NVSS detected samples with angular resolution of 45 arcsec, there are unresolved sources in our catalog. Shabala & Godfrey (2013) have recently investigated the effect of source size in the jet power estimation of Equation 3. They found the dependence on the source size is the power of 0.58 ± 0.17 . Thus, the effect of the source size is expected to be small in the jet power estimation, although it might affect the power estimates for ultra-compact or largely extended sources.

Since our samples are quasars, L_{disk} can be related to

Table 1. Results of Correlation Analysis

x	y	z	Objects	Samples	$\rho_{xy,z}$ ^a	p-value
$\log L_{2500 \text{ \AA}}$	$\log L_{1.4 \text{ GHz}}$	z	SDSS-NVSS quasars ^b	7017	0.39	$< 10^{-10}$
$\log L_{\text{disk}}$	$\log P_{\text{jet}}$	z	SDSS-NVSS quasars ^b	7017	0.40	$< 10^{-10}$
$\log L_{\text{disk}}$	$\log P_{\text{jet}}$	$\log M_{\text{BH}}$	SDSS-NVSS quasars ^b	7017	0.63	$< 10^{-10}$
$\log M_{\text{BH}}$	$\log L_{\text{disk}}$	$\log P_{\text{jet}}$	SDSS-NVSS quasars ^b	7017	0.37	$< 10^{-10}$
$\log M_{\text{BH}}$	$\log P_{\text{jet}}$	$\log L_{\text{disk}}$	SDSS-NVSS quasars ^b	7017	-0.028	0.019
$\log \lambda$	$\log r$	-	SDSS-NVSS quasars ^c	8436	-0.11	$< 10^{-10}$
$\log \lambda$	$\log r$	$\log L_{\text{disk}}$	SDSS-NVSS quasars ^c	8436	-0.022	0.065
$\log L_{\text{disk}}$	$\log P_{\text{jet}}$	z	SDSS-NVSS-WENSS quasars ^b	2077	0.31	$< 10^{-10}$
$\log L_{\text{disk}}$	$\log P_{\text{jet}}$	z	uniform SDSS-NVSS quasars ^b	3545	0.37	$< 10^{-10}$
$\log L_{\text{disk}}$	$\log P_{\text{jet}}$	z	SDSS-NVSS quasars ^d	6081	0.39	$< 10^{-10}$
$\log L_{\text{disk}}$	$\log P_{\text{jet}}$	z	SDSS-NVSS quasars ^e	3083	0.63	$< 10^{-10}$

^aSpearman’s rank correlation coefficient.

^bRadio-loud objects only, $R \geq 10$.

^cAll the SDSS-NVSS quasars are included.

^dThe matching radius is set to be 15 arcsec.

^e $R \geq 100$.

the mass accretion rate \dot{M}_{in} onto the SMBH as

$$L_{\text{disk}} = \epsilon \dot{M}_{\text{in}} c^2, \quad (4)$$

where ϵ is the accretion disk radiative efficiency and c is the speed of light. [Figure 4](#) shows the correlation between the bolometric disk luminosity L_{disk} and the jet power P_{jet} in the logarithmic space. The top and bottom panel shows the histogram of $\log(L_{\text{disk}})$ and $\log(P_{\text{jet}})$, respectively. The linear regression line, shown by the solid line, is given as

$$\log P_{\text{jet}} = (0.96 \pm 0.012) \log L_{\text{disk}} + (0.79 \pm 0.55), \quad (5)$$

where errors show 1σ uncertainties, with a scatter of 0.54. We perform a partial correlation analysis to test the correlation between the $\log L_{\text{disk}}$ and $\log P_{\text{jet}}$ excluding the redshift dependence ([Table 1](#)). The Spearman rank correlation gives $\rho_{LP,z} = 0.40$ with the p-value of $< 10^{-10}$. Therefore, there is a positive correlation between disk luminosity and jet power in radio quasars. We note that, in this paper, we do not include radio non-detected data in the analysis. The effect of such censored data is discussed in [Appendix A](#).

The jet production efficiency is defined as

$$\eta_{\text{jet}} \equiv \frac{P_{\text{jet}}}{\dot{M}_{\text{in}} c^2} = \frac{P_{\text{jet}}}{L_{\text{disk}}/\epsilon}. \quad (6)$$

The dashed line in [Figure 4](#) represents $P_{\text{jet}} = L_{\text{disk}}/\epsilon = \dot{M}_{\text{in}} c^2$ with $\epsilon = 0.1$ corresponding to $\eta_{\text{jet}} = 1$. The distribution of the jet production efficiency of our radio

quasar samples are shown in [Figure 5](#). We show the cases of $\epsilon = 0.1$ and 0.3, although the efficiency can be from 0.057 for a Schwarzschild BH to 0.42 for an extreme Kerr BH (e.g. [Kato et al. 1998](#)). Here, $\langle \log \eta_{\text{jet}} \rangle = -1.97 \pm 0.54$ corresponding to $\eta_{\text{jet}} \simeq 1.1_{-0.76}^{+2.6} \times 10^{-2}$ for $\epsilon = 0.1$. Only 2 quasars have $\eta_{\text{jet}} \geq 1$. This low jet production efficiency is consistent with the study by [van Velzen & Falcke \(2013\)](#) in which they used a correlation between optical and radio luminosities of 763 FR-II quasars utilizing the SDSS-FIRST catalog. This low efficiency is not significantly enhanced even if we set $\epsilon = 0.3$ ([Figure 5](#)).

Connection between the spin value and radiative efficiency is theoretically established for standard accretion disk. It comes from energetics of particles on marginally stable orbits and gives efficiency of radiation production. At large spins, a fraction of radiation is captured by the central BH itself. In this case, the observed efficiency would become lower. Furthermore, innermost portions of the disk is dominated by magnetic fields in the magnetically arrested disk (MAD; [Narayan et al. 2003](#)) framework which is the current leading scenario for the powerful jet launching mechanism (see [subsection 5.6](#) for details). Although their radiative efficiency is expected to be different from that for standard disks, the exact value of the efficiency is still under debate (see e.g., [Punsly 2014, 2015; Punsly et al. 2016; Avara et al. 2016](#)). Considering these uncertainties, we fix $\epsilon = 0.1$ in this paper.

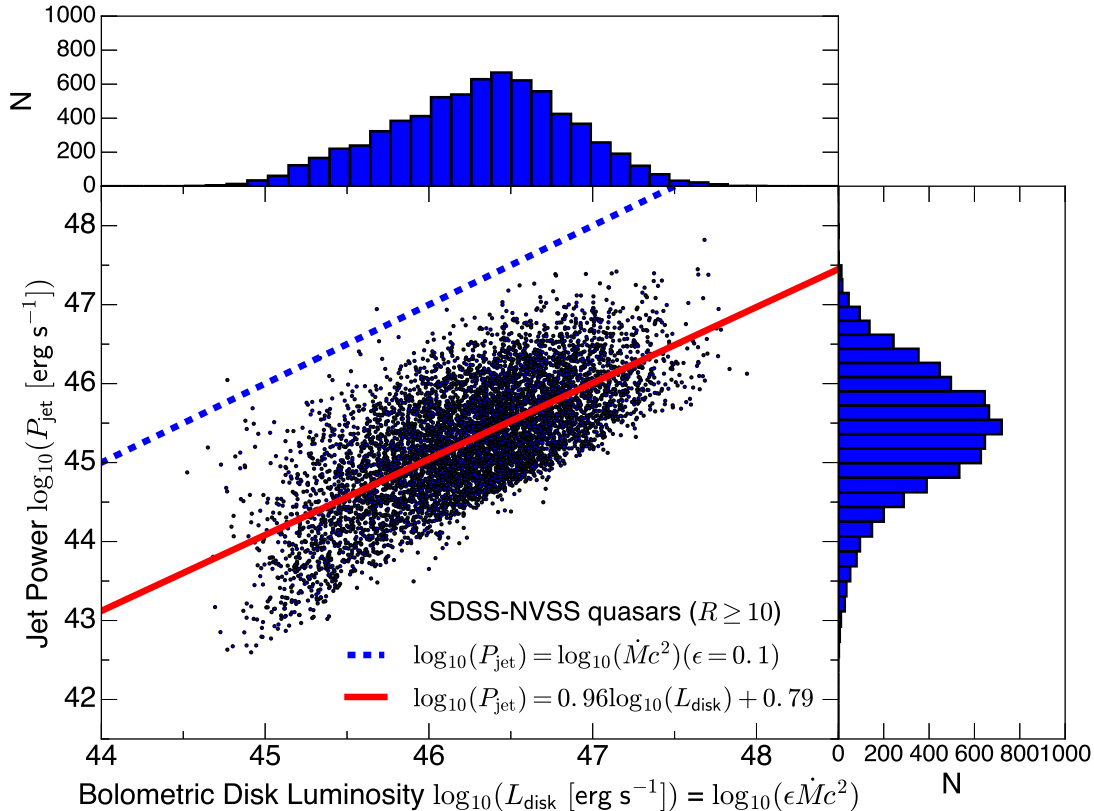


Figure 4. Bolometric disk luminosity vs. jet power of our SDSS–NVSS sample, where the top and right panels show the bolometric disk luminosity and jet power histograms. The solid line gives a linear fit to the data (see Equation 5) with a scatter of 0.74. The dashed line shows the case with the jet production efficiency $\eta_{\text{jet}} = 1$ assuming the disk efficiency $\epsilon = 0.1$.

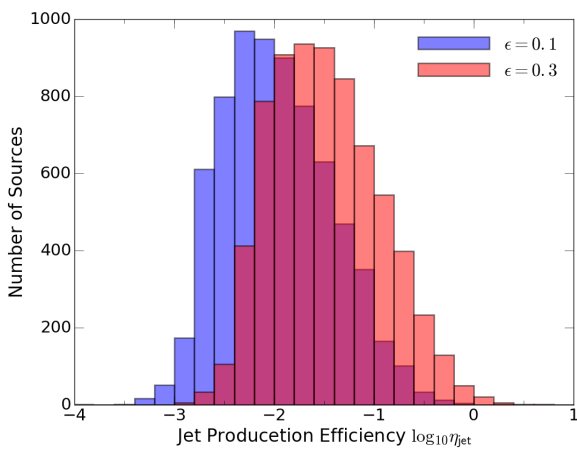


Figure 5. Distribution of the jet production efficiencies of our radio quasar samples. We assume the radiative efficiency of the disk ϵ to be 0.1 (blue) and 0.3 (red).

4. FUNDAMENTAL PLANES IN SUPERMASSIVE BLACK HOLES

Low-accretion rate BH systems ($\lambda \lesssim 0.03$) have been believed to have a fundamental plane among mass, disk

luminosity, and jet power (e.g. Terashima & Wilson 2003; Merloni et al. 2003; Maccarone et al. 2003; Plotkin et al. 2012), while the existence of a fundamental plane for objects accreting at high rates is not well established.

Merloni et al. (2003) established a fundamental plane in stellar mass and supermassive black hole systems using mass, radio luminosity, and X-ray luminosity. With ~ 150 samples, they found that the radio luminosity is correlated with both the BH mass and the X-ray luminosity. However, the SMBH disk luminosity is dominated in optical bands rather than in X-rays (Elvis et al. 1994). And, they used the radio luminosity of the core component only rather than the extended component which includes the whole energy budget of the jet. In this section, we examine the fundamental plane in the SMBH systems with our 7017 radio-loud quasar samples having $\lambda \gtrsim 0.01$.

We examine the mass dependence of the correlation between L_{disk} and P_{jet} (Figure 4). The Spearman rank correlation gives $\rho_{LP,M} = 0.63$ with the p-value of $< 10^{-10}$. Therefore, the positive correlation between disk luminosity and jet power still exist, even if we consider the dependence on the BH mass.

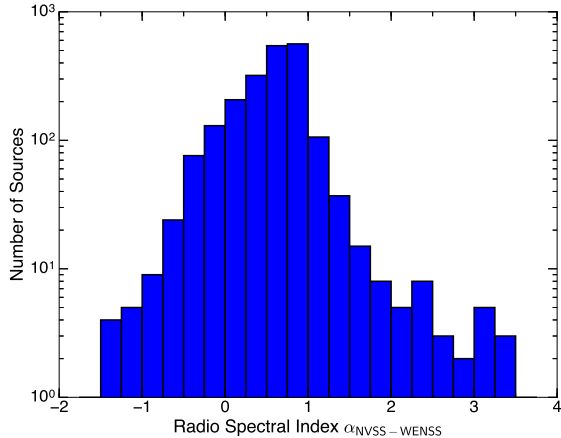


Figure 6. Distribution of the radio spectral index $\alpha_{\text{NVSS-WENSS}}$ between 1.4 GHz (NVSS) and 325 MHz (WENSS) of our SDSS–NVSS–WENSS detected quasar sample.

The correlations between M_{BH} and L_{disk} or P_{jet} are also examined. For the correlation between M_{BH} and L_{disk} , the Spearman rank correlation also gives $\rho_{ML,P} = 0.37$ with the p-value of $< 10^{-10}$. On the contrary, for the correlation between M_{BH} and P_{jet} , the Spearman rank correlation gives $\rho_{MP,L} = -0.028$ with the p-value of 0.019. Thus, once we exclude the dependence on L_{disk} , there is no correlation between M_{BH} and P_{jet} in radio-loud luminous quasars. Therefore, the disk luminosity correlates with both the BH mass and the jet power, while the jet power correlates with the disk luminosity, i.e. absolute mass accretion rate, but not with the BH mass. This result is consistent with semi-analytical studies of SMBH growth (Merloni & Heinz 2008).

The multivariate regression analysis can give the following forms of fitting equations

$$\log L_{\text{disk}} = (23.8 \pm 0.23) + (0.43 \pm 5.5 \times 10^{-3}) \log P_{\text{jet}} + (0.33 \pm 9.4 \times 10^{-3}) \log M_{\text{BH}}, \quad (7)$$

$$\log P_{\text{jet}} = (7.4 \pm 0.54) + (0.84 \pm 1.3 \times 10^{-2}) \log L_{\text{disk}} + (-0.057 \pm 1.5 \times 10^{-2}) \log M_{\text{BH}}. \quad (8)$$

The scatter of each function is 0.37 and 0.59 for Equation 7 and Equation 8, respectively. Here, we note that the correlation between P_{jet} and M_{BH} is not statistically established as discussed above. And, the slope coefficient of $\log M_{\text{BH}}$ term is small as -0.057 implying very weak dependence.

5. DISCUSSIONS

5.1. Effect of Spectral Index

In this paper, we have assumed that the radio spectral index is uniformly $\alpha = 0.8$. However, individual sources

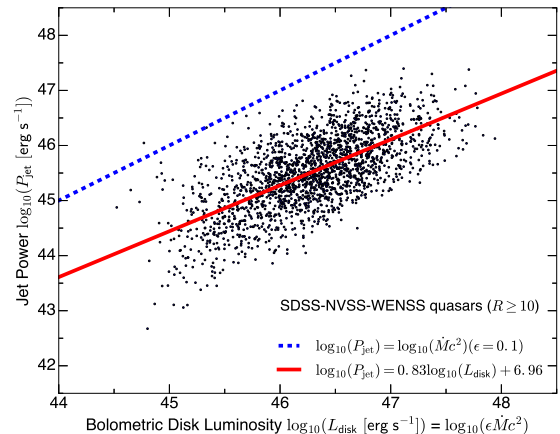


Figure 7. Same as Figure 4, but for the SDSS–NVSS–WENSS detected quasar sub-sample.

would have different spectral indices, which might affect the results (e.g., Yuan et al. 2016, for the radio luminosity function). In this section, we consider the effect of spectral index distribution on estimating the disk–jet correlation.

The unified radio object catalog (Kimball & Ivezić 2008; Kimball & Ivezić 2014) combined five radio catalogs and the optical SDSS survey catalog. Thus, this combined catalog provides the flux information of NVSS sources at different frequencies. Since Equation 3 is calibrated at 151 MHz, we need a lower frequency flux density information for NVSS sources. The unified catalog includes the catalog by the Westerbork Northern Sky Survey (WENSS; Rengelink et al. 1997) at 325 MHz. It covers the sky north of $\delta = 29^\circ$ with a limiting flux of ~ 18 mJy and a beam size of $54'' \times 54'' \csc(\delta)$. The positional accuracy is $\lesssim 1.5''$ for bright sources and $\lesssim 5''$ for faint sources.

The number of the SDSS–NVSS–WENSS detected radio-loud quasar sample is 2077 applying the same matching radius as our parent sample. We use the NVSS source position for the radio source position. Spectral index of individual object is estimated as

$$\alpha_{\text{NVSS-WENSS}} = -\frac{\log(F_{\text{NVSS}}/F_{\text{WENSS}})}{\log(1.4 \text{ GHz}/0.325 \text{ GHz})}, \quad (9)$$

where we use the integrated flux density for radio fluxes. Figure 6 shows the distribution of the spectral index. The distribution has $\langle \alpha_{\text{NVSS-WENSS}} \rangle = 0.57 \pm 0.50$, while we assume $\alpha = 0.8$ for the main sample.

Figure 7 shows the correlation between L_{disk} and P_{jet} of our SDSS–NVSS–WENSS detected quasar sub-sample in the logarithmic space. The regression line, shown by the solid line, is given as

$$\log P_{\text{jet}} = (0.83 \pm 0.020) \log L_{\text{disk}} + (7.0 \pm 0.94), \quad (10)$$

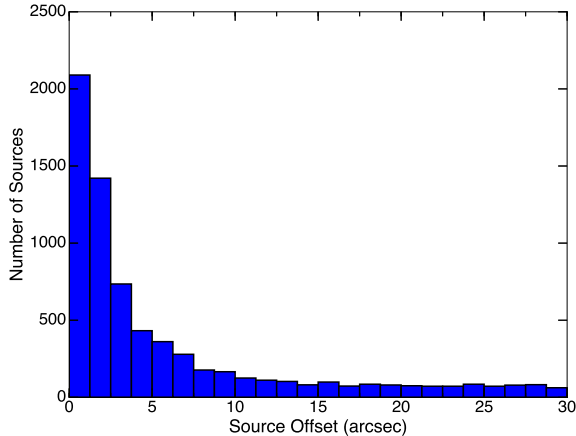


Figure 8. Source offset distribution between the SDSS object and the NVSS object.

with a scatter of 0.51. The Spearman rank correlation gives $\rho_{LP,z} = 0.31$ with the p-value of $< 10^{-10}$. Therefore, there is still a positive correlation between disk luminosity and jet power in radio quasars. Based on the jet production efficiency arguments above, here we have $\langle \log \eta_{\text{jet}} \rangle = -1.86 \pm 0.53$ assuming $\epsilon = 0.1$. Therefore, our results are not changed even if we take into account individual source spectral index variation.

5.2. Different Sensitivity Limits

The primary SDSS DR7 quasar catalog does not provide a uniform catalog due to a variety of criteria for target selection (Shen et al. 2011). Therefore, Shen et al. (2011) provided a catalog flag representing the uniformity of the sample. “Uniform flag = 1” gives a uniformly selected quasar samples with a flux limit of $i = 19.1$ at $z < 2.9$ and $i = 20.2$ at $z > 2.9$ based on the target selection algorithm in Richards et al. (2002). Faint source detection in the NVSS catalog may also suffers from such a completeness problem. Here, the $5\text{-}\sigma$ detection sensitivity limit of NVSS is 2.5 mJy (e.g. Condon et al. 1998; Kimball & Ivezić 2008).

To check such sample selection bias effects, we restrict our samples to the uniformly selected SDSS quasars with $5\text{-}\sigma$ detection at the NVSS band. The resulting number of samples is 3545 radio-loud quasars. The relation between P_{jet} and L_{disk} is given as

$$\log P_{\text{jet}} = (1.1 \pm 0.017) \log L_{\text{disk}} + (-4.8 \pm 0.78), \quad (11)$$

with a scatter of 0.53. The Spearman rank correlation gives $\rho_{LP,z} = 0.37$ with the p-value of $< 10^{-10}$. And, we have $\langle \log \eta_{\text{jet}} \rangle = -2.03 \pm 0.53$. Therefore, our results do not change even if we take into account the uniformity of the sample.

5.3. Matching Radius

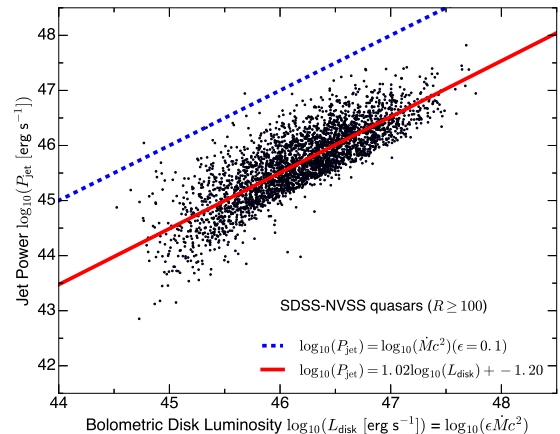


Figure 9. Same as Figure 4, but $R \geq 100$.

In this paper, we match the NVSS radio sources and the DR7 quasar catalog with a matching radius of 30 arcsec and select the closest sources between the catalogs. However, unrelated objects may be matched in our catalog. Figure 8 shows the distribution of the offset between the NVSS and SDSS positions. 84% of objects have the offsets smaller than 15 arcsec. The fraction becomes $\gtrsim 90\%$ for the offsets of ≤ 20 arcsec. Therefore, the fraction of the mismatched objects would be minor in our parent catalog (Best et al. 2005).

We restrict our samples to the SDSS–NVSS quasars with the matching radius of 15 arcsec to consider the selection effect by the matching radius. This sub-sample contains 6081 radio-loud objects. The relation between P_{jet} and L_{disk} with the matching radius of 15 arcsec is given as

$$\log P_{\text{jet}} = (0.94 \pm 0.013) \log L_{\text{disk}} + (1.8 \pm 0.60), \quad (12)$$

with a scatter of 0.54. The Spearman rank correlation gives $\rho_{LP,z} = 0.39$ with the p-value of $< 10^{-10}$. Therefore, the correlation between disk luminosity and jet power still statistically exists. The jet production efficiency is given as $\langle \log \eta_{\text{jet}} \rangle = -1.93 \pm 0.54$.

5.4. Effect of Radio Loudness Cut

At $10 \leq R \lesssim 100$, radio-loud quasars are also called as radio-intermediate quasars (Falcke et al. 1996). Most of them are likely to be FR-I type radio quasars. Figure 9 shows the correlation between L_{disk} and P_{jet} of the SDSS–NVSS detected quasars but having $R \geq 100$. The dashed line represent $P_{\text{jet}} = \dot{M}_{\text{in}} c^2$. 3083 quasars are included. The regression line, shown by the solid line, is given as

$$\log P_{\text{jet}} = (1.0 \pm 0.013) \log L_{\text{disk}} + (-1.2 \pm 0.59), \quad (13)$$

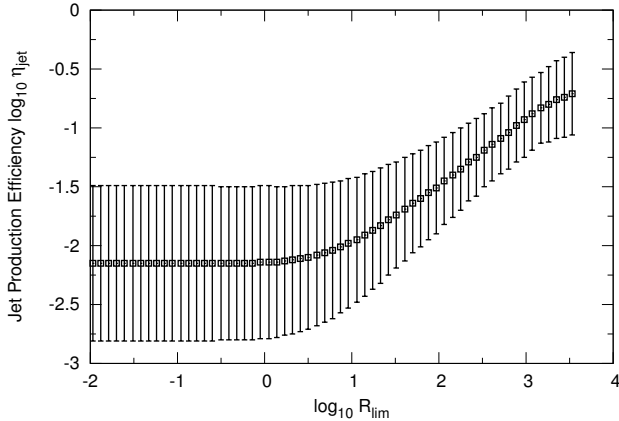


Figure 10. Jet production efficiency η_{jet} as a function of the limiting radio loudness R_{lim} . $1\text{-}\sigma$ statistical uncertainty of the data is also shown.

with a scatter of 0.38. The Spearman rank correlation gives $\rho_{LP,z} = 0.63$ with the p-value of $< 10^{-10}$. There is still a positive correlation between disk luminosity and jet power in radio quasars. Based on the jet production efficiency arguments above, here we have $\langle \log \eta_{\text{jet}} \rangle = -1.49 \pm 0.38$. By selecting sources at $R \geq 100$, a slightly higher jet production efficiency is expected but still be consistent with that at $R \geq 10$ at the $1\text{-}\sigma$ level.

Figure 10 shows the estimated jet production efficiency as a function of the limiting radio loudness. As we select high jet power objects by setting high R_{lim} , the jet production efficiency gradually increases with R_{lim} . However, even at $R_{\text{lim}} \gtrsim 10^3$, η_{jet} is still at an order of 0.1.

5.5. Comparison with Blazar Studies

The relation between disk and jet has been also investigated using blazar spectral fitting studies (e.g. Celotti & Ghisellini 2008; Ghisellini et al. 2014; Inoue & Tanaka 2016). Different from our radio quasar studies, blazar studies enable us to compare accretion with jet outflow at the same epoch. Multi-wavelength observations from radio to gamma-ray allow us to study overall SED and physical parameters of jets via spectral fitting. A spectrum of a blazar is composed of two emission components: the low-energy component is synchrotron radiation and the other one is inverse Compton component targeting synchrotron radiation (e.g. Jones et al. 1974; Maraschi et al. 1992) and/or external radiation field (e.g. Dermer & Schlickeiser 1993; Sikora et al. 1994).

Generally, blazar spectral fitting studies predict large jet production efficiencies $\eta_{\text{jet}} \sim 0.1\text{--}10$ (e.g. Celotti & Ghisellini 2008; Ghisellini et al. 2014; Inoue & Tanaka 2016), while our results show $\eta_{\text{jet}} \simeq 1.1_{-0.76}^{+2.6} \times 10^{-2}$. Such a difference has also been recently reported by Pjanka et al. (2016) using published blazar samples.

Here, the jet power estimates based on blazar spectral fittings strongly rely on the assumptions on the pair fraction and the electron minimum Lorentz factor $\gamma_{e,\text{min}}$ (see e.g. Inoue & Tanaka 2016; Pjanka et al. 2016). More pairs per one proton and/or higher $\gamma_{e,\text{min}}$ would reduce the jet power estimation based on blazar spectral fit. Although γ_{min} is known to be $\sim m_p/m_e$ for the terminal shocks of quasar jets (Stawarz et al. 2007), the minimum Lorentz factor of electrons in blazar jet is not well constrained. Recent *NuSTAR* observations revealed that electron spectrum extends down to electron energies of at least $\gamma_e \sim 10^2 - 10^3$ for nearby BL Lacs (Kataoka & Stawarz 2016; Madejski et al. 2016). If γ_{min} is determined by the mass ratio of a proton and an electron (i.e. $\gamma_{\text{min}} = m_p/m_e$), the jet power can be an order of one to two lower than the case in which γ_{min} is determined by the energy ratio between protons and electrons (Inoue & Tanaka 2016), which would lead a consistent result with our radio quasar studies.

5.6. Implication on to the Jet Production

Recent general relativistic magnetohydrodynamic (GRMHD) numerical studies showed that powerful relativistic jets are launched in the MAD which can confine magnetic flux on BHs by its ram pressure (Tchekhovskoy et al. 2011; McKinney et al. 2012). Extracted jet power by the rotation of BHs threaded by magnetic fields, so-called the BZ power, is given by (Blandford & Znajek 1977; Tanabe & Nagataki 2008; Tchekhovskoy et al. 2010, 2011)

$$P_{\text{BZ}} = 4.0 \times 10^{-3} \frac{1}{c} \Omega_{\text{H}}^2 \Phi_{\text{BH}}^2 f(\Omega_{\text{H}}) \quad (14)$$

$$\simeq 10 \left(\frac{\phi_{\text{BH}}}{50} \right)^2 x_a^2 f(x_a) \dot{M}_{\text{in}} c^2, \quad (15)$$

where $\Omega_{\text{H}} = ac/2r_{\text{H}}$ is the angular frequency of the BH horizon, Φ_{BH} is the net magnetic field flux accumulated in the central region, $x_a \equiv r_g \Omega_{\text{H}}/c$, and $f(x_a) \approx 1 + 1.38x_a^2 - 9.2x_a^4$. $a \equiv J_{\text{BH}}/J_{\text{BH,max}} = cJ_{\text{BH}}/GM_{\text{BH}}^2$ is the dimensionless BH spin parameter, $r_{\text{H}} = r_g(1 + \sqrt{1 - a^2})$ is the horizon radius, $r_g = GM_{\text{BH}}/c^2$ is the gravitational radius of the BH. $\phi_{\text{BH}} = \Phi_{\text{BH}}/\sqrt{\dot{M}_{\text{in}} r_g^2 c}$ is the dimensionless magnetic flux threading the BH and is typically on the order of 50 based on GRMHD simulations (McKinney et al. 2012)². This gives $\eta_{\text{jet,BZ}} \equiv P_{\text{BZ}}/\dot{M}_{\text{in}} c^2 \simeq 10(\phi_{\text{BH}}/50)^2 x_a^2 f(x_a)$.

Figure 11 gives the distribution of the dimensionless spin parameter a assuming $\epsilon = 0.1$ and $\phi_{\text{BH}} = 50$.

² In McKinney et al. (2012), the dimensionless magnetic flux is denoted by $\Upsilon_{\text{BH}} \approx \Phi_{\text{BH}}/5\sqrt{\dot{M}_{\text{in}} r_g^2 c} = \phi_{\text{BH}}/5$ (Gammie 1999; Penna et al. 2010). Typically, Υ_{BH} is the order of 10 (see Table 9 in McKinney et al. 2012).

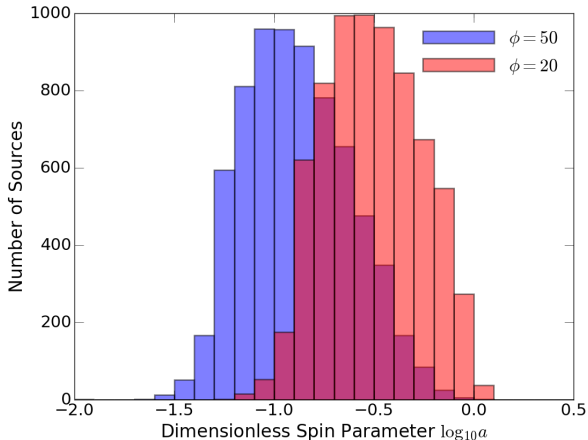


Figure 11. Distribution of the dimensionless spin parameters of our radio quasar samples. The dimensionless magnetic flux ϕ_{BH} is set to be 50 (blue) and 20 (red). We assume the radiative efficiency of the disk ϵ to be 0.1.

For $\phi_{\text{BH}} = 50$, $\langle \log a \rangle = -0.88 \pm 0.26$ corresponding to $a \simeq 0.13^{+0.11}_{-0.059}$. However, this spin parameter value is smaller than what is expected from the cosmological merger SMBH evolution models (Volonteri et al. 2005, 2007, 2013). Figure 11 also shows the spin parameter distribution but assuming $\phi_{\text{BH}} = 20$. In this case, we have $\langle \log a \rangle = -0.50 \pm 0.24$. Therefore, the results on the spin parameter strongly depend on the assumption on the magnetic flux threading the BH which is expected to be the dominant factor for the generation of jets considering the radio loudness distribution (Sikora & Begelman 2013).

Observationally, various attempts have been recently considered to measure the magnetic field near active SMBHs. VLBI observations toward M 87, whose accretion rate is significantly sub-Eddington (Di Matteo et al. 2003), revealed $B \sim 10$ G at the jet base $\sim 10R_s$ from the central BH using the synchrotron self-absorption (SSA) frequency (Kino et al. 2015; Hada et al. 2016). Recent linear polarimetric adaptive optics observation of an AGN torus yields a dusty torus magnetic field strength in the range of 4–82 mG assuming a clumpy torus model (Lopez-Rodriguez et al. 2015). Maser observations also constrains the magnetic fields at ~ 0.2 pc from the central BH to be $\lesssim 1$ G (Gnedin et al. 2014). Although the B-field in the inner region (near the corona scale) has not been well investigated yet, future detection of coronal synchrotron emission would provide an information on magnetic field (Inoue & Doi 2014; Raginski & Laor 2016). Possible millimeter excess has been already reported from a nearby radio-quiet AGN NGC 985 (Doi & Inoue 2016). If this excess is coming from the corona, the magnetic field strength at 100 times the Schwarzschild radius is expected to be ~ 150 G

(Doi & Inoue 2016) near the equipartition value with the gas energy density. Assuming $\epsilon = 0.1$, this yields $\phi_{\text{corona}} \sim 2$. If ϕ_{BH} is such a low value even for radio quasars, faster spin parameters are required.

Avara et al. (2016) have recently found that the jet production efficiency in the MAD scenario depend not only on the spin and magnetic flux but also on the geometrical thickness of the accretion flow. Geometrical thickness of the accretion from our quasar samples is expected to be small since they are at the range of $0.01 \lesssim \lambda_{\text{disk}} \lesssim 0.3$ (See Figure 1). However, the disk structure itself is not well understood. In the MAD scenario, the disk is expected to be truncated at the outer radius of a magnetospheric radius (Narayan et al. 2003). Although we would be able to locate the inner radius based on Iron-K line analysis (George & Fabian 1991), it is still not clear whether there is any systematic trend of disk truncation in radio-loud AGNs. Some radio-loud AGNs show the inner radius is $> 10R_s$ (e.g., Larsson et al. 2008; Sambruna et al. 2009; Tazaki et al. 2010; Tombesi et al. 2011; Tazaki et al. 2013), while the disks of others extend down to $\sim 4-6R_s$ (Kataoka et al. 2007; Sambruna et al. 2011).

5.7. Radio Loudness and Disk Eddington Ratio

The correlation between λ and R (Figure 1) is also another important indicator for the disk and jet connection. Sikora et al. (2007) found a negative correlation between the radio loudness R and the Eddington accretion ratio by covering nearly 7 orders of magnitude in disk Eddington ratios. And, a clear bimodality is seen in the correlation (Sikora et al. 2007), although Broderick & Fender (2011) pointed out that the bimodality becomes less apparent when R is determined from the core luminosity only and a mass correction is applied (see also Gardner & Done 2014). The physical origin of the correlation between λ and R is still under debate.

The correlation can be tested with our full quasar sample (Figure 1), although our sample covers only about 3 orders of magnitude in disk Eddington ratios ($0.01 \lesssim \lambda \lesssim 1$). The Spearman rank correlation gives $\rho_{\lambda R} = -0.11$ with the p-value of $< 10^{-10}$. Therefore, a negative correlation between λ and R exists at $0.01 \lesssim \lambda \lesssim 1$. Here, both R and λ depend on the disk luminosity. If L_{disk} is set as the control variable, $\rho_{\lambda R, L}$ becomes -0.022.

This weak negative correlation between R and λ can be fitted by the function of

$$\log R = (-0.28 \pm 0.015) \log \lambda + (1.5 \pm 0.015), \quad (16)$$

with a scatter of 0.74. Following the MAD scenario (Narayan et al. 2003), it is expected to be $R \propto \eta_{\text{jet}}/\epsilon \propto \lambda^{-0.4}$ (Sikora et al. 2013). Although we find $R \propto \lambda^{-0.28}$, distributions of M_{BH} and magnetic fluxes would cause

dispersion on this relation. [Sikora et al. \(2013\)](#) argued that R can decrease with increasing λ if all cold accretion episodes start after the magnetic flux accumulation by a hot (geometrically thick) accretion phase. Indications of such a process during the Bondi accretion phase have been recently provided by studies of $P_{\text{jet}}/\dot{M}_{\text{Bondi}}$ in nearby radio galaxies ([Nemmen & Tchekhovskoy 2015](#)). [Rusinek et al. \(2016\)](#) proposed that time variation would cause this trend. The jet power estimated in this paper is time-averaged values, while the disk luminosity is the instantaneous value as discussed above. Since our sample covers only $0.01 \lesssim \lambda \lesssim 1$, additional samples covering lower λ are necessary for more detailed analysis on this relation.

6. CONCLUSIONS

In this paper, we studied the disk-jet connection in active SMBHs utilizing 7017 SDSS-NVSS detected radio-loud quasars up to $z = 4.9$. We converted the 1.4 GHz radio luminosity to the jet power using an empirical relation ([Willott et al. 1999](#)) which is calibrated by the X-ray cavity measurements ([Willott et al. 1999](#); [Godfrey & Shabala 2013](#)). Bolometric accretion disk luminosity is estimated by the SED templates in [Richards et al. \(2006\)](#). Central BH mass is also provided by [Shen et al. \(2011\)](#) using a single-epoch spectrum.

We found that the quasar jet powers correlate with the bolometric disk luminosities. We have $\log P_{\text{jet}} = (0.96 \pm 0.012) \log L_{\text{disk}} + (0.79 \pm 0.55)$ with a scatter of 0.54. The jet power rarely exceeds the accretion luminosity. By assuming the accretion disk efficiency of $\epsilon = 0.1$, we further found that the jet production efficiency is $\eta_{\text{jet}} \simeq 1.1_{-0.76}^{+2.6} \times 10^{-2}$. These results do not significantly change even if we adopt various different selection criteria or the higher disk efficiency of $\epsilon = 0.3$. η_{jet} gradually increases with the limiting radio loudness, although it will be still at an order of 0.1 even for $R_{\text{lim}} \gtrsim 10^3$.

We further tested the existence of the fundamental plane among M_{BH} , L_{disk} , and P_{jet} for quasars at $0.01 \lesssim \lambda$. We could not find a statistically significant correlation between M_{BH} and P_{jet} excluding the dependence on L_{disk} . This implies that the plane would not exist for radio-loud quasars in the standard accretion regime. This is consistent with recent studies which revealed that the plane exists only for low accretion AGNs (e.g. [Merloni & Heinz 2008](#); [Plotkin et al. 2012](#)).

The relation between radio loudness, R , and the disk Eddington ratio λ is also investigated. Our samples cover about 3 orders of magnitude in λ . With our large sample, we confirmed that there is a weak negative correlation between R and λ . This is consistent with the report in [Sikora et al. \(2007\)](#). However, our samples covered only at $10^{-2} \lesssim \lambda \lesssim 10$. Future deeper optical spectroscopic surveys such as the Subaru Prime Focus

Spectrograph survey ([Takada et al. 2014](#); [Sugai et al. 2015](#)) would help us to extend our samples to optically faint AGNs, i.e. high radio-loudness objects.

Following the BZ scenario ([Blandford & Znajek 1977](#)), the jet power is related to the BH spin and the magnetic flux threading the BH. Taking the value of the dimensionless magnetic flux value from numerical simulations by [McKinney et al. \(2012\)](#) $\phi_{\text{BH}} = 50$, we estimated the distribution of the dimensionless spin parameters a . However, the resulting a is $\simeq 0.13_{-0.059}^{+0.11}$ which is much smaller than what is expected from the cosmological merger SMBH evolution (e.g., [Volonteri et al. 2013](#)). Therefore, the magnetic flux strength threading the SMBHs might be weaker than it is expected from numerical simulations following the spin evolutionary models. Magnetic field measurements in the vicinity of the central BHs would help us to understand the detailed BZ processes. The resulting low jet efficiency can be also due to dependence of the efficiency on geometrical thickness of the accretion flow ([Avara et al. 2016](#)), since our quasar samples accreting at $0.01 \lesssim \lambda_{\text{disk}} \lesssim 0.3$ is expected to be have small geometrical thickness.

The authors thank Chris Done, Hirokazu Odaka, and Andreas Schulze for useful comments and discussions. The authors also thank the anonymous referee for his/her useful and constructive comments which improved the paper a lot. YI is supported by the JAXA international top young fellowship and JSPS KAKENHI Grant Number 420 JP16K13813. STSDAS is a product of the Space Telescope Science Institute, which is operated by AURA for NASA.

Funding for the SDSS and SDSS-II has been provided by the Alfred P. Sloan Foundation, the Participating Institutions, the National Science Foundation, the U.S. Department of Energy, the National Aeronautics and Space Administration, the Japanese Monbukagakusho, the Max Planck Society, and the Higher Education Funding Council for England. The SDSS Web Site is <http://www.sdss.org/>. The SDSS is managed by the Astrophysical Research Consortium for the Participating Institutions. The Participating Institutions are the American Museum of Natural History, Astrophysical Institute Potsdam, University of Basel, University of Cambridge, Case Western Reserve University, University of Chicago, Drexel University, Fermilab, the Institute for Advanced Study, the Japan Participation Group, Johns Hopkins University, the Joint Institute for Nuclear Astrophysics, the Kavli Institute for Particle Astrophysics and Cosmology, the Korean Scientist Group, the Chinese Academy of Sciences (LAMOST), Los Alamos National Laboratory, the Max-Planck-Institute for Astronomy (MPIA), the Max-Planck-Institute for Astrophysics (MPA), New Mexico State University, Ohio

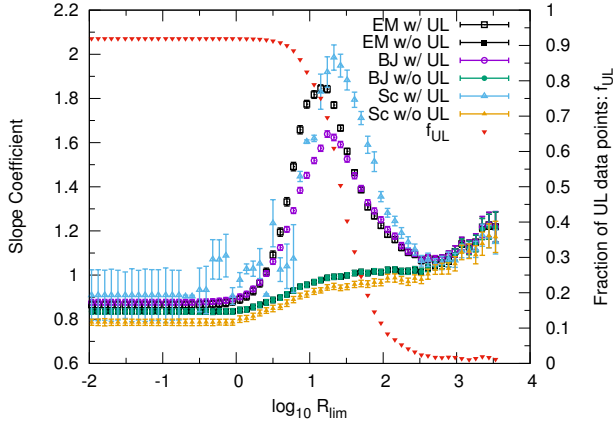


Figure A1. Slope coefficient of the regression line between L_{disk} and P_{jet} as a function of limiting radio loudness R_{lim} . Open data treat only detected samples, while filled data include censored data. Square, circle, and upper-triangle corresponds to the results from the expectation-maximization (EM) algorithm, the Buckley-James (BJ) algorithm, and the Schmitt’s (Sc) algorithm, respectively. The down-triangle points show the number fraction of non-detected samples.

State University, University of Pittsburgh, University of Portsmouth, Princeton University, the United States Naval Observatory, and the University of Washington.

Facilities: NVSS, SDSS, WENSS

APPENDIX

A. CORRELATION ANALYSIS WITH CENSORED DATA

In this paper, we use only detected data. However, our samples are flux-limited samples. Given the SDSS DR7 quasar catalog, a portion of those quasars are not detected in NVSS. Such a censored data set would affect the results and implication to the data (e.g. [Isobe et al. 1986](#); [Bonchi et al. 2013](#)). In this section, we argue how the results will be affected by such a censored data.

The number of the SDSS DR7 quasars is 105783 ([Shen et al. 2011](#)), while our parent sample contains 8436 SDSS-DR7 quasars of which 7017 are radio-loud. Since it is known that only about 10% of quasars are radio-loud ([Baloković et al. 2012](#)), this large difference is naturally expected. Therefore, if we include all the SDSS DR7 quasar, radio data are dominated by the upper limits of unrelated radio-quiet objects whose radio emission is generated by quasar driven disk outflows rather than relativistic jets (e.g. [Zakamska & Greene 2014](#)). In order to investigate radio-loud objects, we restrict samples above a certain radio-loudness R_{lim} . For non-detected objects, we can select sources by setting the upper lim-

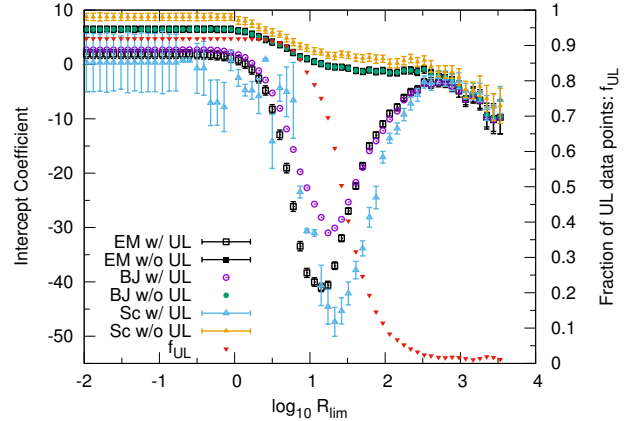


Figure A2. Same as [Figure A1](#), but showing intercept coefficients.

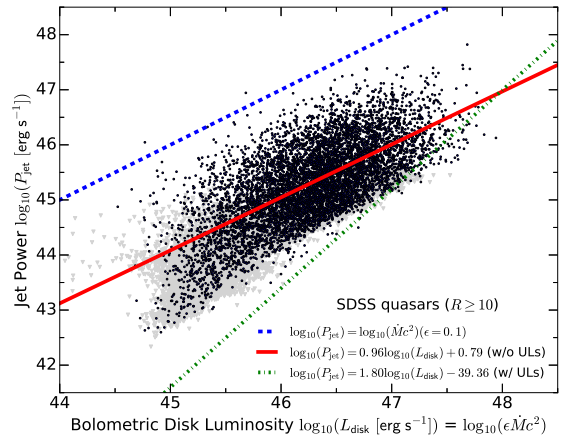


Figure A3. Same as [Figure 4](#), but including censored data (gray triangles). Regression line including the censored data is shown in dot-dashed. The EM algorithm is adopted.

its on the radio loudness R_{UL} above R_{lim} , where radio flux upper limits for non-detected objects are set as the detection limit of the NVSS, 2.5 mJy ([Condon et al. 1998](#)).

[Figure A1](#) and [Figure A2](#) show the slope coefficient and the intercept coefficient, respectively, in the regression analysis of the $(L_{\text{disk}}, P_{\text{jet}})$ plane as a function of R_{lim} for the data sets with and without non-detected objects. We adopt the three regression analysis methods; expectation-maximization (EM) algorithm, the Buckley-James (BJ) algorithm, and the Schmitt’s (Sc) algorithm. The EM algorithm is similar to the least-squares fitting method, and assumes that the intrinsic residuals of P_{jet} are normally distributed in log space about the regression line for fixed values of L_{disk} . Censored data are taken into account by determining the degree to which the upper limits are compatible with the

assumed dispersion about the regression line. The BJ algorithm is similar in approach, but uses the Kaplan-Meier distribution for the residuals. The Sc method divides the (x, y) plane into bins and uses the Kaplan-Meier distribution for the residuals. [Isobe et al. \(1986\)](#) provide details about these algorithms.

The three regression algorithms give similar results for the entire the R_{lim} range. However, it is clear that the results becomes significantly different by the treatment of non-detection data samples, specifically at $\log R_{\text{lim}} \lesssim 2.5$ where the fraction of non-detected data starts to increase. In order to see how the results are affected by censored data, [Figure A3](#) shows the relation between L_{disk} and P_{jet} setting $R \geq 10$ including censored data. The regression line for the detected sources is given in [Equation 5](#), while the regression line incorporating the censored data is given in

$$\log P_{\text{jet}} = (1.80 \pm 0.017) \log L_{\text{disk}} + (-39.4 \pm 0.81), \quad (\text{A1})$$

with a scatter of 1.10. The values are from the EM method assuming a normal distribution for the residuals. It is clearly seen that the regression line for the censored data does not well reproduce the detected data.

In the fitting procedure in the methods above, regression lines for the censored data generally become lower than the original upper limit (UL) values. This is because censored data are incorporated determining the degree to which the upper limits are compatible with the assumed dispersion about the regression line. The expected true values of the censored data from the regression analysis could become lower than the UL values. Thus, the true value of R of the UL data would become $< R_{\text{lim}}$. However, we need to restrict samples having $R \geq R_{\text{lim}}$ in order to select objects having relativistic jets. This inconsistency potentially leads spurious outcomes by taking into account the censored data. Thus, in order to avoid such results due to unrelated datasets, we do not include the censored data in our analysis.

REFERENCES

- Avara, M. J., McKinney, J. C., & Reynolds, C. S. 2016, *MNRAS*, 462, 636
- Baade, W., & Minkowski, R. 1954, *ApJ*, 119, 215
- Baloković, M., Smolčić, V., Ivezić, Ž., et al. 2012, *ApJ*, 759, 30
- Baum, S. A., & Heckman, T. 1989, *ApJ*, 336, 702
- Becker, R. H., White, R. L., & Helfand, D. J. 1995, *ApJ*, 450, 559
- Best, P. N., Kauffmann, G., Heckman, T. M., & Ivezić, Ž. 2005, *MNRAS*, 362, 9
- Blandford, R. D., & McKee, C. F. 1982, *ApJ*, 255, 419
- Blandford, R. D., & Znajek, R. L. 1977, *MNRAS*, 179, 433
- Blundell, K. M., & Rawlings, S. 2000, *AJ*, 119, 1111
- Bonchi, A., La Franca, F., Melini, G., Bongiorno, A., & Fiore, F. 2013, *MNRAS*, 429, 1970
- Brenneman, L. W., Reynolds, C. S., Nowak, M. A., et al. 2011, *ApJ*, 736, 103
- Broderick, J. W., & Fender, R. P. 2011, *MNRAS*, 417, 184
- Buttiglione, S., Capetti, A., Celotti, A., et al. 2010, *A&A*, 509, A6
- Celotti, A., & Ghisellini, G. 2008, *MNRAS*, 385, 283
- Condon, J. J., Cotton, W. D., Greisen, E. W., et al. 1998, *AJ*, 115, 1693
- Dermer, C. D., & Schlickeiser, R. 1993, *ApJ*, 416, 458
- Di Matteo, T., Allen, S. W., Fabian, A. C., Wilson, A. S., & Young, A. J. 2003, *ApJ*, 582, 133
- Doi, A., & Inoue, Y. 2016, *PASJ*, 68, 56
- Elvis, M., Wilkes, B. J., McDowell, J. C., et al. 1994, *ApJS*, 95, 1
- Fabian, A. C. 2012, *ARA&A*, 50, 455
- Falcke, H., Sherwood, W., & Patnaik, A. R. 1996, *ApJ*, 471, 106
- Fanaroff, B. L., & Riley, J. M. 1974, *MNRAS*, 167, 31P
- Fukugita, M., Ichikawa, T., Gunn, J. E., et al. 1996, *AJ*, 111, 1748
- Gammie, C. F. 1999, *ApJL*, 522, L57
- Gardner, E., & Done, C. 2014, *MNRAS*, 438, 779
- George, I. M., & Fabian, A. C. 1991, *MNRAS*, 249, 352
- Ghirlanda, G., Ghisellini, G., Tavecchio, F., Foschini, L., & Bonnoli, G. 2011, *MNRAS*, 413, 852
- Ghisellini, G., Tavecchio, F., Maraschi, L., Celotti, A., & Sbarrato, T. 2014, *Nature*, 515, 376
- Gnedin, Y. N., Globina, V. N., Piotrovich, M. Y., Buliga, S. D., & Natsvlshvili, T. M. 2014, *Astrophysics*, 57, 163
- Godfrey, L. E. H., & Shabala, S. S. 2013, *ApJ*, 767, 12
- Grandi, S. A., & Osterbrock, D. E. 1978, *ApJ*, 220, 783
- Gunn, J. E., Siegmund, W. A., Mannery, E. J., et al. 2006, *AJ*, 131, 2332
- Hada, K., Kino, M., Doi, A., et al. 2016, *ApJ*, 817, 131
- Inoue, Y. 2011, *ApJ*, 733, 66
- Inoue, Y., & Doi, A. 2014, *PASJ*, 66, L8
- Inoue, Y., & Tanaka, Y. T. 2016, *ApJ*, 828, 13
- Isobe, T., Feigelson, E. D., & Nelson, P. I. 1986, *ApJ*, 306, 490
- Jones, T. W., O'dell, S. L., & Stein, W. A. 1974, *ApJ*, 188, 353
- Kaspi, S., Smith, P. S., Netzer, H., et al. 2000, *ApJ*, 533, 631
- Kataoka, J., & Stawarz, L. 2016, *ApJ*, 827, 55
- Kataoka, J., Reeves, J. N., Iwasawa, K., et al. 2007, *PASJ*, 59, 279
- Kato, S., Fukue, J., & Mineshige, S., eds. 1998, *Black-hole accretion disks*
- Katz, J. I. 1976, *ApJ*, 206, 910
- Kimball, A., & Ivezić, Z. 2014, *ArXiv e-prints*, arXiv:1401.1535
- Kimball, A. E., & Ivezić, Ž. 2008, *AJ*, 136, 684
- King, A. L., Miller, J. M., Gültekin, K., et al. 2013, *ApJ*, 771, 84
- Kino, M., Takahara, F., Hada, K., et al. 2015, *ApJ*, 803, 30
- Komissarov, S. S., Barkov, M. V., Vlahakis, N., & Königl, A. 2007, *MNRAS*, 380, 51
- Kozieł-Wierzbowska, D., & Stasińska, G. 2011, *MNRAS*, 415, 1013
- Krawczyk, C. M., Richards, G. T., Mehta, S. S., et al. 2013, *ApJS*, 206, 4
- Larsson, J., Fabian, A. C., Ballantyne, D. R., & Miniutti, G. 2008, *MNRAS*, 388, 1037
- Lavalley, M., Isobe, T., & Feigelson, E. 1992, in *Astronomical Society of the Pacific Conference Series*, Vol. 25, *Astronomical Data Analysis Software and Systems I*, ed. D. M. Worrall, C. Biemesderfer, & J. Barnes, 245
- Liu, Z., Yuan, W., Lu, Y., & Zhou, X. 2015, *MNRAS*, 447, 517
- Lopez-Rodriguez, E., Packham, C., Jones, T. J., et al. 2015, *MNRAS*, 452, 1902
- Lu, Y., Wang, T., Zhou, H., & Wu, J. 2007, *AJ*, 133, 1615
- Maccarone, T. J., Gallo, E., & Fender, R. 2003, *MNRAS*, 345, L19

- Madejski, G. M., Nalewajko, K., Madsen, K. K., et al. 2016, ArXiv e-prints, arXiv:1609.02203
- Maraschi, L., Ghisellini, G., & Celotti, A. 1992, *ApJL*, 397, L5
- Martínez-Sansigre, A., & Rawlings, S. 2011, *MNRAS*, 414, 1937
- McKinney, J. C., Tchekhovskoy, A., & Blandford, R. D. 2012, *MNRAS*, 423, 3083
- McLure, R. J., & Dunlop, J. S. 2001, *MNRAS*, 327, 199
- . 2004, *MNRAS*, 352, 1390
- Merloni, A., & Heinz, S. 2008, *MNRAS*, 388, 1011
- Merloni, A., Heinz, S., & di Matteo, T. 2003, *MNRAS*, 345, 1057
- Moriyama, K., & Mineshige, S. 2015, *PASJ*, 67, 106
- Mullin, L. M., Riley, J. M., & Hardcastle, M. J. 2008, *MNRAS*, 390, 595
- Narayan, R., Igumenshchev, I. V., & Abramowicz, M. A. 2003, *PASJ*, 55, L69
- Nemmen, R. S., & Brotherton, M. S. 2010, *MNRAS*, 408, 1598
- Nemmen, R. S., & Tchekhovskoy, A. 2015, *MNRAS*, 449, 316
- Osterbrock, D. E. 1977, *ApJ*, 215, 733
- O’Sullivan, E., Giacintucci, S., David, L. P., et al. 2011, *ApJ*, 735, 11
- Padovani, P. 1992, *A&A*, 256, 399
- Pâris, I., Petitjean, P., Aubourg, É., et al. 2014, *A&A*, 563, A54
- Penna, R. F., McKinney, J. C., Narayan, R., et al. 2010, *MNRAS*, 408, 752
- Peterson, B. M. 1993, *PASP*, 105, 247
- Pjanka, P., Zdziarski, A. A., & Sikora, M. 2016, ArXiv e-prints, arXiv:1607.08895
- Plotkin, R. M., Markoff, S., Kelly, B. C., Körding, E., & Anderson, S. F. 2012, *MNRAS*, 419, 267
- Pozdniakov, L. A., Sobol, I. M., & Siuniaev, R. A. 1977, *Soviet Ast.*, 21, 708
- Punsly, B. 2014, *ApJL*, 797, L33
- . 2015, *ApJ*, 806, 47
- Punsly, B., Reynolds, C., Marziani, P., & O’Dea, C. P. 2016, *MNRAS*, 459, 4233
- Raginski, I., & Laor, A. 2016, *MNRAS*, 459, 2082
- Rawlings, S., & Saunders, R. 1991, *Nature*, 349, 138
- Rawlings, S., Saunders, R., Eales, S. A., & Mackay, C. D. 1989, *MNRAS*, 240, 701
- Rengelink, R. B., Tang, Y., de Bruyn, A. G., et al. 1997, *A&AS*, 124, doi:10.1051/aas:1997358
- Richards, G. T., Fan, X., Newberg, H. J., et al. 2002, *AJ*, 123, 2945
- Richards, G. T., Lacy, M., Storrie-Lombardi, L. J., et al. 2006, *ApJS*, 166, 470
- Runnoe, J. C., Brotherton, M. S., & Shang, Z. 2012, *MNRAS*, 422, 478
- Rusinek, K., Sikora, M., Koziel-Wierzbowska, D., & Godfrey, L. 2016, Submitted
- Sambruna, R. M., Tombesi, F., Reeves, J. N., et al. 2011, *ApJ*, 734, 105
- Sambruna, R. M., Reeves, J. N., Braito, V., et al. 2009, *ApJ*, 700, 1473
- Saunders, R., Baldwin, J. E., Rawlings, S., Warner, P. J., & Miller, L. 1989, *MNRAS*, 238, 777
- Schneider, D. P., Richards, G. T., Hall, P. B., et al. 2010, *AJ*, 139, 2360
- Shabala, S. S., & Godfrey, L. E. H. 2013, *ApJ*, 769, 129
- Shen, Y., Richards, G. T., Strauss, M. A., et al. 2011, *ApJS*, 194, 45
- Sikora, M., & Begelman, M. C. 2013, *ApJL*, 764, L24
- Sikora, M., Begelman, M. C., & Rees, M. J. 1994, *ApJ*, 421, 153
- Sikora, M., Stasińska, G., Koziel-Wierzbowska, D., Madejski, G. M., & Asari, N. V. 2013, *ApJ*, 765, 62
- Sikora, M., Stawarz, L., & Lasota, J.-P. 2007, *ApJ*, 658, 815
- Stawarz, L., Cheung, C. C., Harris, D. E., & Ostrowski, M. 2007, *ApJ*, 662, 213
- Sugai, H., Tamura, N., Karoji, H., et al. 2015, *Journal of Astronomical Telescopes, Instruments, and Systems*, 1, 035001
- Sunyaev, R. A., & Titarchuk, L. G. 1980, *A&A*, 86, 121
- Takada, M., Ellis, R. S., Chiba, M., et al. 2014, *PASJ*, 66, R1
- Takahashi, H. R., Ohsuga, K., Kawashima, T., & Sekiguchi, Y. 2016, *ApJ*, 826, 23
- Tanabe, K., & Nagataki, S. 2008, *PhRvD*, 78, 024004
- Tazaki, F., Ueda, Y., Ishino, Y., et al. 2010, *ApJ*, 721, 1340
- Tazaki, F., Ueda, Y., Terashima, Y., Mushotzky, R. F., & Tombesi, F. 2013, *ApJ*, 772, 38
- Tchekhovskoy, A., Narayan, R., & McKinney, J. C. 2010, *ApJ*, 711, 50
- . 2011, *MNRAS*, 418, L79
- Terashima, Y., & Wilson, A. S. 2003, *ApJ*, 583, 145
- Tombesi, F., Sambruna, R. M., Reeves, J. N., Reynolds, C. S., & Braito, V. 2011, *MNRAS*, 418, L89
- van Velzen, S., & Falcke, H. 2013, *A&A*, 557, L7
- Vestergaard, M. 2002, *ApJ*, 571, 733
- Vestergaard, M., & Peterson, B. M. 2006, *ApJ*, 641, 689
- Volonteri, M., Madau, P., Quataert, E., & Rees, M. J. 2005, *ApJ*, 620, 69
- Volonteri, M., Sikora, M., & Lasota, J.-P. 2007, *ApJ*, 667, 704
- Volonteri, M., Sikora, M., Lasota, J.-P., & Merloni, A. 2013, *ApJ*, 775, 94
- Willott, C. J., Rawlings, S., Blundell, K. M., & Lacy, M. 1999, *MNRAS*, 309, 1017
- Woo, J.-H., & Urry, C. M. 2002, *ApJ*, 579, 530
- York, D. G., Adelman, J., Anderson, Jr., J. E., et al. 2000, *AJ*, 120, 1579
- Yuan, Z., Wang, J., Zhou, M., & Mao, J. 2016, *ApJ*, 829, 95
- Zakamska, N. L., & Greene, J. E. 2014, *MNRAS*, 442, 784
- Zirbel, E. L., & Baum, S. A. 1995, *ApJ*, 448, 521